First International Symposium on Marine Propulsors
smp'09, Trondheim, Norway, June 2009

Computation of hull-pressure fluctuations due to non-cavitating propellers

Frans Hendrik Lafeber, Erik van Wijngaarden, Johan Bosschers
Maritime Research Institute Netherlands (MARIN), Wageningen, The Netherlands

ABSTRACT
This paper describes a new coupling procedure of two boundary element methods aimed at computing propeller-induced hull-pressure fluctuations. The first method computes the incompressible potential flow of a propeller operating in a ship wake field. The second method computes the propeller-radiated pressures by replacing the incompressible-flow solution on the rotating propeller blades by a set of rings of stationary sources. This source system is used as input in an acoustic scattering analysis of the wetted ship hull and undisturbed free surface based on the Kirchhoff-Helmholtz integral equation. Thus, hull pressures are obtained in the frequency domain on the basis of a time-domain source description.

Computed hull pressures for non-cavitating conditions are presented for a container vessel that was successively fitted with two different propellers, one being a six-bladed propeller designed for the vessel, the other a two-bladed propeller. Comparisons are made with scale-model tests performed in a towing tank. For the two-bladed propeller, the computed results are in good agreement with the experimental results. The six-bladed propeller shows somewhat larger variations in correlation.

Keywords
Hull-pressure fluctuations, non-cavitating propellers, boundary element methods, validation experiments.

1 INTRODUCTION
Computation of the pressure field on the hull due to a propeller operating behind a ship is used to assess the excitation forces on the aftship in an early design stage. This hull-pressure field contains components due to the passing blades as well as cavitation and is influenced by the diffraction effect of the wetted ship hull and the free surface. For the computation of the total pressure field all of these contributions should be taken into account. Here, only the computation of the non-cavitating contribution is considered using a few validation experiments.

The advantage of considering only the non-cavitating propeller is that its flow is less difficult to compute than that of the cavitating propeller, and that the variability in the measurement data is much smaller. The prediction of the diffraction effect can thus be assessed at larger accuracy than for a cavitating propeller. Another important issue is that with the reduction in sheet cavity extents on modern propellers, the non-cavitating part becomes of greater practical importance. Often, only the tip vortex is cavitating and the hull-pressure amplitude at the first blade-passage frequency (BPF) is dominated by the contribution from the non-cavitating propeller.

In this paper the hull-pressure fluctuations are computed using a new coupling procedure between two boundary element methods (BEM). The computational approach is described in Section 2. Sections 3 and 4 discuss the experimental and computational procedures. Results of the validation study are described in Section 5.

2 THEORY
In this section, the boundary element codes are briefly described. The method of coupling the two codes by replacing the rotating sources representing the propeller by a set of rings of non-rotating sources is treated in detail. The application of Bernoulli's equation for the determination of the pressure fluctuations is discussed.

2.1 Propeller flow analysis
For the analysis of the flow past a propeller, use is made of a time-domain BEM that solves the incompressible potential flow equations for lifting surfaces, see e.g. Vaz & Bosschers (2006) and Bosschers et al. (2008). The method, designated PROCAL, has been developed within MARIN's Cooperative Research Ships (CRS) for the unsteady analysis of cavitating propellers operating in a prescribed ship wake. The code is a low order BEM that solves for the velocity disturbance potential using the Morino approach. A sheet cavitation model was implemented in which the non-linear kinematic and dynamic boundary conditions are iteratively solved assuming that the cavity surface coincides with the body surface. In the computations presented, the pitch and contraction of the propeller wake geometry are prescribed using empirical formulations, while the strength of the wake is computed using an iterative pressure Kutta condition. The strength of the monopoles and dipoles for each panel on the body and wake is written to file for one revolution.

2.2 Hull-pressure analysis
For the analysis of the diffracted hull pressures induced by the propeller, use is made of a frequency domain BEM that solves the Kirhhoff-Helmholtz integral equation for compressible fluids (van Wijngaarden, 2006). The

method, designated EXCALIBUR, has originally been developed in MARIN's background research program and was recently further developed within CRS. It is a low order BEM code that solves for the acoustic velocity potential using the Burton & Miller approach. Thus, no main flow is taken into account and the free surface is modeled through a negative-mirror-imaging procedure. The diffraction problem is solved for locations on the hull on the basis of a prescribed set of sources. The pressure fluctuations are then obtained by application of Bernoulli's equation discussed in Section 2.4.

2.3 Combining PROCAL and EXCALIBUR

In the past, hull pressures would have been obtained from a simple combination of the two codes described above. EXCALIBUR computed a so-called solid boundary factor (SBF) in the frequency domain. PROCAL would then compute the pressure in the free-field at the location of the hull. By multiplying this free field pressure by the SBF, the pressure on the hull was obtained. However, as discussed by Bosschers et al. (2008), this method has the drawback of modeling the hull-diffraction effect by one monopole only, whereas the source system actually consists of a large set of monopoles and dipoles. A new method is presented here by which the complete solution from PROCAL is used as input for EXCALIBUR. This new method is based on replacing the time domain flow solution on the propeller by a stationary set of rings of monopole and dipole sources in the frequency domain as suggested by Brouwer (2005).

The propeller's elemental sources of noise (i.e. monopoles and dipoles) are rotating around the propeller centre line. This can also be said of the helicoidally shed vorticity; the propeller wake, which consists of only dipoles. Assuming non-uniform, but stationary propeller inflow, the source field becomes periodic in time at BPF, ω_1, given by $\omega_1 = Z\Omega$, with Z the number of propeller blades and Ω the propeller revolution rate in rad/s. Time, T, needed for one revolution is $T = 2\pi/\Omega$. Likewise, $T_1 = 2\pi/Z\Omega = 2\pi/\omega_1$ denotes the blade-passage period. In the following, a procedure is presented for the Fourier transformation of the rotating sources to a set of stationary sources pulsating at BPFs in the frequency domain.

To translate the time-domain solution of sources moving with the propeller from PROCAL to a frequency-domain set of stationary sources for EXCALIBUR, we assume the propeller blades and wake surfaces to be approximated by $N_b + N_w$ panels with panel-collocation points, $\vec{x}_i(t)$, for $i = 1..N_b + N_w$. During one revolution of period T, N_t 'snapshots' are made of the propeller at equidistant intervals of $\Delta t = T / N_t$. The set of time samples in a revolution is indexed $t_j = j\Delta t$ with $j = 0..N_t - 1$. Each of the $N_b + N_w$ collocation points assumes N_t positions, $\vec{x}_i(t_j) = \vec{x}_{ij}$. Also, each of the panels can be associated with a point source of monopole type and strength, $\sigma_i(t_j) = \sigma_{ij}$, plus one of surface normal dipole type and strength, $\mu_i(t_j) = \mu_{ij}$. Note that the trailing vortex sheets consist of only dipole sources.

For brevity of notation, we denote source strengths $\mu_i(t)$ or $\sigma_i(t)$ at a fixed point by $f(t)$. This is the product of the instantaneous strength, which we denote f_{ij}, and a step function that is one during the time step when the panel's collocation point coincides with the source position, and zero at other times. As the number of time steps is always taken as a multiple of the blade number, $N_t = N_{t1}Z$, the step function actually becomes one at Z time steps during one propeller revolution. Now, the $N_b + N_w$ rotating sources are replaced by $(N_b + N_w)N_t$ stationary ones. Then, $f(t)$ can be developed into a Fourier series based on an interval covering one blade passage period, T_1,

$$f(t) = \mathrm{Re}\left\{\sum_n \left(c_n e^{-i\omega_n t}\right)\right\} \tag{1}$$

in which

$$c_n = \frac{2}{T_1}\int_{t_j - T_1/2}^{t_j + T_1/2} f(t) e^{+i\omega_n t} dt \tag{2}$$

with $\omega_n = n\omega_1$ for the n^{th} harmonic and $n \neq 0$. It follows,

$$\begin{aligned} c_n &= 2\frac{f_{ij}}{T_1}\int_{t_j - \Delta t/2}^{t_j + \Delta t/2} e^{+i\omega_n t} dt \\ &= 2 f_{ij}\frac{\Delta t}{T_1} e^{i\omega_n t_j}\frac{\sin(\omega_n \Delta t/2)}{\omega_n \Delta t/2} \\ &= 2 f_{ij}\frac{Z}{N_t} e^{i\omega_n t_j}\mathrm{sinc}\left(\pi n \frac{Z}{N_t}\right) \end{aligned} \tag{3}$$

and hence,

$$f(t) = 2 f_{ij}\frac{Z}{N_t}\mathrm{Re}\left\{\sum_n \mathrm{sinc}\left(\pi n \frac{Z}{N_t}\right) e^{-i\omega_n (t - t_j)}\right\} \tag{4}$$

with $\mathrm{sinc}(x) = \sin(x)/x$. For a certain harmonic order, n, the complex amplitude f_n of source ij is given by

$$f_n = 2 f_{ij}\frac{Z}{N_t}\mathrm{sinc}\left(\pi n \frac{Z}{N_t}\right) e^{+i2\pi n Z j / N_t} \tag{5}$$

The sources with complex amplitudes given by Eq. (5) form the input for EXCALIBUR. The scattering effect of the hull is then computed for harmonics of the BPF. The resulting pressure fluctuations on the hull are given as a real amplitude and phase lead relative to a sine function.

2.4 Application of Bernoulli's equation

Using the unsteady Bernoulli equation, the pressure disturbance p is given by

$$p = i\rho\omega\phi - \rho U\frac{\partial\phi}{\partial x} - \tfrac{1}{2}\rho\left|\vec{\nabla}\phi\right|^2 \tag{6}$$

Where ρ is the density of the fluid, ω is the frequency, ϕ is the disturbance potential and U is the free stream velocity in the direction of the positive x-axis, which is parallel to the ship center line and positive towards the bow. Assuming that the square of the disturbance velocities is small, Eq. (6) is reduced to

$$p = i\rho\omega\phi - \rho U \frac{\partial \phi}{\partial x} \quad (7)$$

When the convective term is neglected as well, we get

$$p = i\rho\omega\phi \quad (8)$$

Eq. (8) is currently applied in EXCALIBUR to compute the complex amplitude of the pressure fluctuations on the hull for harmonics of BPF.

3 EXPERIMENTS

A series of experiments was conducted to provide data to validate the combination of the computer codes PROCAL and EXCALIBUR. For the experiments, a model of a large container vessel was fitted with different propellers, and bollard pull and towing tests were performed. During the bollard pull test, the model was fitted with a large two-bladed stock propeller leading to a tip clearance of 14% of the propeller diameter. The pitch was reduced such that it generated a minimal thrust ($P_{0.7}/D$ = 0.05). This way, only the thickness contribution of the propeller plays a role. For the towing tests, the model was fitted with the six-bladed propeller designed for this ship. The tip clearance of this propeller was 33% of the propeller diameter. The model was towed at various speeds and with different propeller rotation rates, see Table 1, where N_m is the model propeller rotation rate, V_m the model speed, K_T the dimensionless thrust coefficient and D_m the propeller diameter.

Table 1: Model test conditions

Test	Z [-]	N_m [RPM]	BPF [Hz]	V_m [m/s]	K_T [-]	D_m [mm]
A	2	600	20.0	0.00	0.021	340
B	6	579	57.9	2.37	0.204	260
C	6	370	37.0	2.37	-0.010	260

During the tests, the pressure on the hull was measured by means of 21 sensors, which were mounted flush in the area above the propeller, see Figure 1 Figure 2.

The results of the hull pressures are presented as the amplitude and phase of the pressure at the first four harmonics of the BPF. Only the results of the nine pressure sensors close to the propeller are presented: sensors P04-P06, P09-P11 and P14-P16, see Figure 2. The pressure amplitudes at the other sensors were not significant (i.e. smaller than 0.1 kPa full scale equivalent) and have been omitted.

Figure 1: Two-bladed propeller fitted to the ship model equipped with flush-mounted pressure sensors

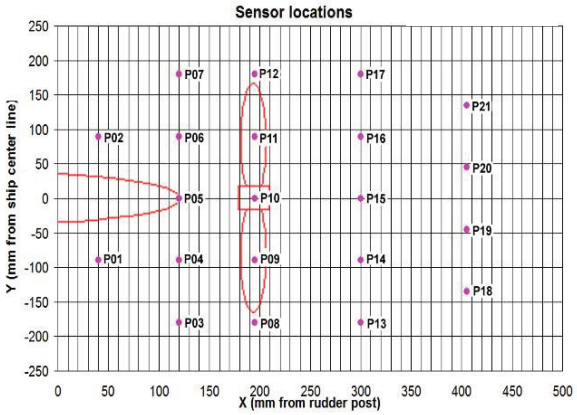

Figure 2: Location of pressure sensors with the propeller and rudder location indicated (dimensions on model scale)

4 COMPUTATIONS

PROCAL computations have been performed at the same propeller rotation rate and thrust coefficient as the model tests. For the bollard pull tests, steady computations were made using uniform inflow. For the towing-test conditions, unsteady computations were performed using the measured ship wake, which was made effective with a force-field method. One propeller revolution is composed of 120 time steps. In the computations presented, 30 panels have been used between the trailing and leading edge of the two-bladed propeller and 40 panels in the case of the six-bladed propeller. In both cases, 20 panels were used between root and tip. Cavitation features have not been considered for the current investigation.

The PROCAL result was then used as input for the EXCALIBUR computations, as described in Section 2.3. Only the aft part of the ship was modeled without the rudder and the draught was increased by the dynamic trim. A total of 1300 panels was used to describe the hull geometry. All computations were performed at model scale. Figure 3 gives an example of a combined PROCAL and EXCALIBUR solution.

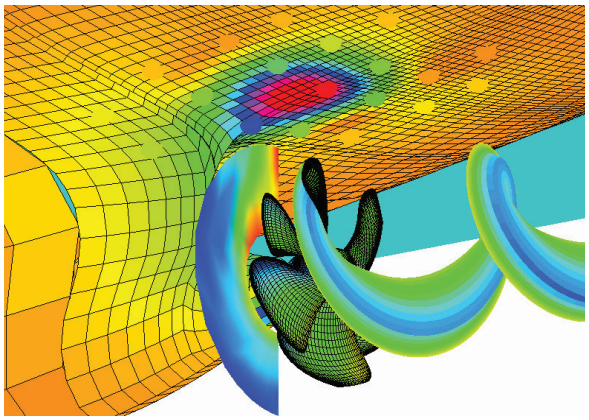

Figure 3: Example of computational result: propeller with ship wake, propeller wake (one blade) and pressure field on the hull. Dots on the hull indicate measuring locations.

5 RESULTS

A comparison between the computations and model test results can now be made for all three tests presented in Table 1. The measured and computed pressure amplitudes are shown for the nine pressure sensors as stated in Section 3. Of the computed phase, only the error is shown. The error in phase (lead) is given by

$$\varepsilon_{phase} = \alpha_{computed} - \alpha_{measured} \tag{9}$$

By dividing this error by the harmonic order n and the number of blades Z, the error relative to the angular blade position in the ship wake is obtained,

$$\varepsilon_{relative} = \varepsilon_{phase} / nZ \tag{10}$$

Using the phase and amplitude of the first four harmonics, a time series can be reconstructed of both the computational and experimental data,

$$p(t) = \sum_{n=1}^{4} A_n \left(\sin n\omega_1 t + \alpha_n \right) \tag{11}$$

At time $t = 0$ the propeller's generator line goes through top dead center.

5.1 Test A

The results of the two-bladed propeller (diameter 340 mm) show a good agreement between computation and experiment. As can be seen in Figure 4, the amplitude at the first harmonic is predicted well, especially for the transducers in the propeller plane. For the higher harmonics of test A (not shown), the error in amplitude increases slightly. In Figure 5 it can be seen that the phase of the first harmonic is computed quite accurately as well. The small error is almost constant across the sensors.

The relative error remains of the same order of magnitude (~7°) for all harmonics. The time series of one propeller revolution is shown in Figure 6 for pressure sensor P10, which is located straight above the propeller. The shapes of the time series are very similar from which it can be concluded that the 2nd, 3rd and 4th harmonics are computed accurately as well. The small constant offset in phase is also visible. Summarizing, the results for the two-bladed propeller with almost no inflow and a low thrust are very good. This indicates that the contribution of the propeller thickness to the diffracted hull-pressure field is properly captured.

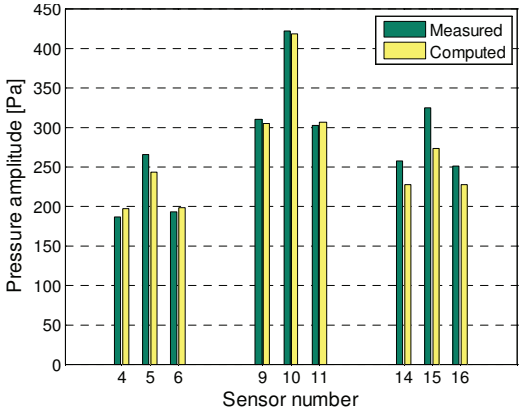

Figure 4: Computed and measured amplitudes for 1st harmonic of test A

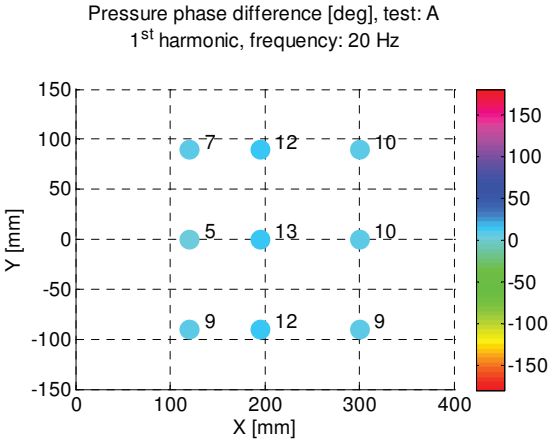

Figure 5: Error in phase, 1st harmonic, test A

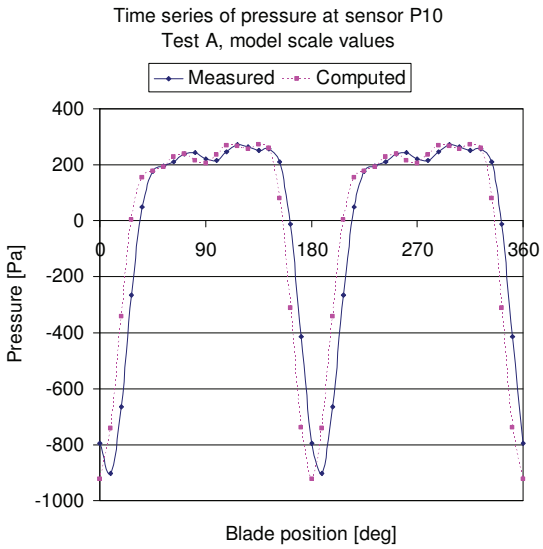

Figure 6: Time series reconstructed from the first four harmonics, test A

5.2 Test B

For the six-bladed propeller (diameter 260 mm) at the design K_T, the computed and measured amplitude and phase show a reasonable agreement directly above the propeller at the first harmonic, see Figure 7 and Figure 8.

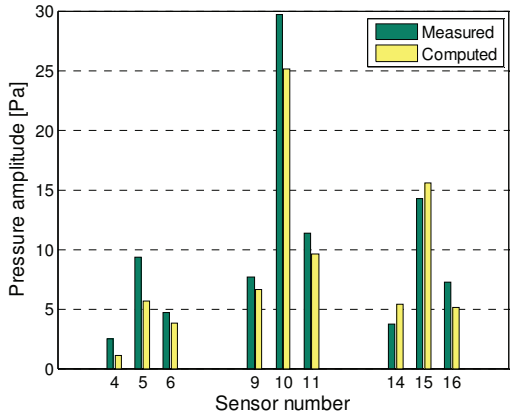

Figure 7: Computed and measured amplitudes for 1st harmonic of test B

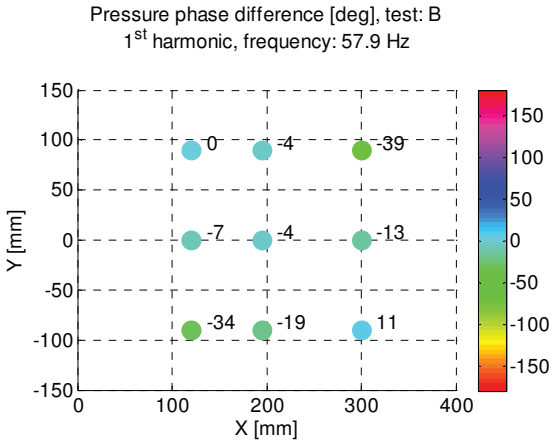

Figure 8: Error in phase, 1st harmonic, test B

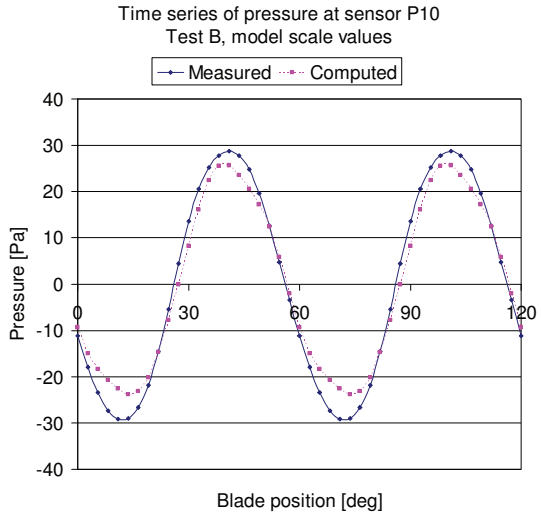

Figure 9: Time series reconstructed from the first four harmonics, test B

At the higher harmonics, all sensors show insignificant amplitudes. This can also be seen in the reconstructed time series which is an almost perfect sine (see Figure 9 in which only two blade passages have been plotted). The error in amplitude and relative phase error remain almost constant for the higher harmonics.

5.3 Test C

In test C, the thrust coefficient of the six-bladed propeller was reduced to almost zero by reducing the rotation rate of the propeller. Again, the largest errors are seen at the sensors with very low amplitudes, see Figure 10. Directly above the propeller, the amplitude error is small: +3% of the measured value. The distributions of the pressures for the upcoming and downgoing blades are not predicted well.

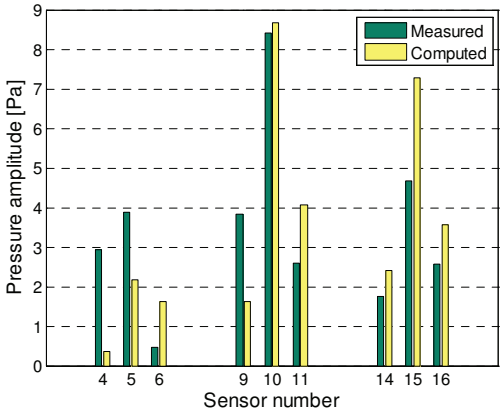

Figure 10: Computed and measured amplitudes for 1st harmonic of test C

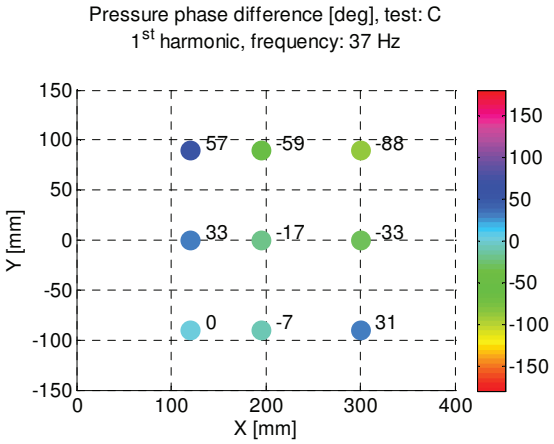

Figure 11: Error in phase, 1st harmonic, test C

In test C, the error in the phase is larger than in test B (Figure 11). As was seen before, the sensors with a low pressure amplitude also give the largest errors in the computed phase. When reconstructing the time series for test C, the errors in amplitude and phase become clearly visible, see Figure 12. Especially the pressures at the higher harmonics are not computed accurately.

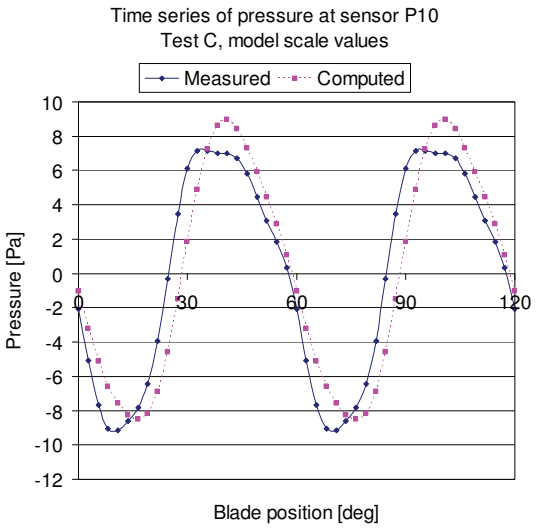

Figure 12: Time series reconstructed from the first four harmonics, test C

5.4 Discussion of the results

The fact that the two-bladed propeller showed more accurate results than the six-bladed might be explained by the omission of the convective term in Bernoulli's equation; compare Eqs.(7) and (8). A first estimate of this term revealed that it can influence the computed amplitude by 10% to 15% and the phase by 5 to 10 degrees. For the case of the two-bladed propeller, including the convective term will not change the results since the inflow velocity U is almost zero.

Another possible cause of deviations between the computations and the measurements is the fact that the flow vorticity is only coarsely modeled in the BEM. Leading edge vortices as well as the roll-up of the tip vortex are not properly captured. This may explain the less accurate prediction of the six-bladed propeller where in the zero load condition, large pressure peaks at the leading edge on the face of the propeller were observed in the computations. These pressure peaks suggest the presence of a leading edge vortex in the measurements.

6 CONCLUSIONS

A new coupling procedure has been presented of two boundary element methods aimed at computing propeller-induced hull-pressure fluctuations. The first method computes the incompressible potential flow of a propeller operating in a ship wake field. The second method computes the propeller-radiated pressures by replacing the incompressible flow solution on the rotating propeller blades by a set of rings of stationary sources. Thus, hull-pressures are computed in the frequency domain on the basis of a time-domain source description.

The method has been evaluated using experimental data obtained in a towing basin for a single-screw ship hull equipped with a two-bladed and a six-bladed propeller, both operating in non-cavitating conditions. For the two-bladed propeller, the computed hull-pressure fluctuations show good agreement with the experiments. In the case of the six-bladed propeller at the design loading, the computed results are reasonable to good. However, when the loading is reduced to a value of almost zero the differences between computations and experiments increase.

The general conclusion is that the combination of the two boundary element methods gives a reasonable to good prediction of the pressures on the hull of a ship due to a non-cavitating propeller. Further improvements are expected by including the convective term in Bernoulli's equation. The influence of the propeller wake and tip vortex model used in the boundary element method needs to be further studied, especially for off-design conditions.

ACKNOWLEDGEMENTS

The present work was partly funded by the Cooperative Research Ships (CRS). The graphical user interface (used for Figure 3) was developed within CRS by DRDC Atlantic, with Dave Heath as main developer. The authors also like to acknowledge the contributions made by Herman Beeksma of MARINs software development department.

REFERENCES

Bosschers, J., Vaz, G., Starke, A.R. & Wijngaarden, E. van (2008). 'Computational analysis of propeller sheet cavitation and propeller-ship interaction', Marine CFD 2008, Southampton, United Kingdom

Brouwer, J. (2005). Ship propeller-induced noise and vibrations, M.Sc. Thesis, University of Twente, Enschede, The Netherlands

Vaz, G., Bosschers, J., (2006). 'Modelling three dimensional sheet cavitation on marine propellers using a boundary element method', CAV 2006 Sixth International Symposium on Cavitation, Wageningen, The Netherlands

Wijngaarden, E. van (2006). 'Determination of propeller source strength from hull-pressure measurements', Proceedings of the 2nd international ship & noise conference 2006, London, United Kingdom